J. Phys. Soc. Japan 30, 228 (1971).
[14]R. M. Macfarlane, Phys. Rev. B 1, 989 (1970).
[15]H. Böhm, Ann. Physik 32, 521 (1938).
[16]D. L. Kraus and G. C. Nutting, J. Chem. Phys. 9, 133 (1941).
[17]Harold P. Klug, J. Am. Chem. Soc. 62, 2992 (1940).
[18]Klug is not in agreement with Lipson (Ref. 4) if it is assumed that substitution of Cr^{3+} for Al^{3+} leaves the structure unchanged. Lipson finds for $XAl(SO_4)_2 \cdot 12H_2O$, α type for $X=K$, NH_4, Tl, and Rb, and β type for $X=Cs$ and NH_3CH_3.
[19]Naoki Koshizuka, Tishirō Ban, and Ikuji Tsujikawa, J. Phys. Soc. Japan 30, 470 (1971).
[20]C. Ancenot and L. Couture, J. Phys. (Paris) 21, 47 (1960).
[21]Julian Eisenstein, Rev. Mod. Phys. 24, 74 (1952).

PHYSICAL REVIEW B VOLUME 6, NUMBER 3 1 AUGUST 1972

Metallic-Field Effect and Its Consequences in Field Emission, Field Ionization, and the Capacitance of a Capacitor

A. K. Theophilou and A. Modinos
Department of Electrical Engineering, The University of Salford, Salford M5 4WT, United Kingdom
(Received 29 November 1971)

The metallic-field effect at a metal surface is calculated in a semi-self-consistent manner using an approximate version of Bardeen's method for the evaluation of the surface potential barrier. The consequences of the metallic-field effect in relation to field emission, field ionization, and the capacitance of a parallel-plate capacitor are considered. In field emission this produces, at high fields, a small deviation from the Fowler-Nordheim formula towards lower currents. In field ionization it leads to increased ion current and a narrower energy distribution. It has no significant effect on the capacitance of a capacitor.

I. INTRODUCTION

The penetration of an externally applied field into a metal at a metal-vacuum interface is of interest in problems of field ionization and field desorption,[1,2] in field emission,[2,3] and in relation to the capacitance of a thin-plate capacitor.[2,4] The similar problem of metal field "penetration" at a metal-insulator interface is of interest in relation to the capacitance and tunneling characteristics of a thin film (less than 30 Å or so) sandwiched between two metal electrodes.[5,6]

Tsong and Muller[2] attempted an evaluation of the field penetration factor at a metal-vacuum interface using the Thomas-Fermi model in a manner analogous to the one used for treating field penetration in semiconductors.[7] The Thomas-Fermi model is supplemented by the boundary condition that the electrostatic potential is such that $dV/dx = F$ at the metal-vacuum interface taken at $x=0$ (F denotes the applied electric field). However, the Thomas-Fermi model is expected to give good results when the induced potential varies slowly over an electron wavelength. This is in fact the case in semiconductors, because of the small free-electron density and the consequent large penetration of the electric field. It is hardly the case with a metal, where as a result of the comparatively high free-electron density at the metal-vacuum interface, one gets a small penetration of the electric field. Moreover, the boundary condition $dV/dx = F$ at a mathematical metal-vacuum interface is a restrictive one because it assumes an abrupt termination of the electronic charge density at the interface and in a proper calculation it must be replaced by

$$\lim_{x\to\infty} \frac{dV^{el}}{dx} = F \ .$$

In practice it will be sufficient to assume that the limiting value is acquired a few angstroms away from a mathematical metal-vacuum interface, which we shall define more precisely in Sec. II. As we shall see this may lead in the case of a metal to qualitatively different conclusions. Other authors[3,8,9] studied field penetration using a linear response formalism within the random-phase approximation (RPA) and assuming an infinite potential barrier at the surface. Again the imposition of the boundary condition $dV^{el}/dx = F$ at a sharply defined metal-vacuum interface is a serious disadvantage of these calculations. The use of the RPA may also be very difficult to justify in the present problem. In particular, the assumption of a linear dielectric response to the externally applied field could be a disadvantage. Our results have shown that nonlinear effects are significant in this region.

In this paper we present an approximate semi-self-consistent calculation which avoids the abrupt boundary condition at $x=0$. Section II contains the basic assumptions and the method of numerical calculation.

In Sec. III we give an approximate analytical estimate of the field penetration which avoids lengthy numerical calculations. The full numerical results based on the method of Sec. II are given in Sec. IV. Applications to field emission, field ionization, and to the capacitance of a thin-plate capacitor are discussed in Sec. V.

II. BASIC ASSUMPTIONS AND METHOD OF CALCULATIONS

A model for the calculation of the electronic properties at the surface of a neutral metal has been originally suggested by Bardeen[10] in connection with the evaluation of the electric dipole-layer contribution to the work function of sodium. According to this model the metal is taken to be semi-infinite, extending from $-\infty$ along the x axis to a metal-vacuum interface in the neighborhood of the origin ($x=0$). The positive ions are replaced by a uniform positive background which extends from $-\infty$ to $x=0$, where it terminates abruptly. The electronic charge distribution, on the other hand, spreads beyond the positive background edge into vacuum thus creating an electrostatic dipole-layer contribution to the surface potential barrier and the work function for the metallic electrons. The total potential barrier that the electron sees consists, to a larger extent, of an exchange (plus correlation) interaction with the other electrons and the electrostatic potential energy mentioned above. Except for the correlation effect (which can be treated very approximately) the potential barrier can be calculated self-consistently for the above model and this has been done by Bardeen to a certain degree of approximation. In the case of the neutral metal the electronic wave functions satisfy the Hartree-Fock equations:

$$\frac{-\hbar^2}{2m}\nabla^2\psi^0_{\vec{K}}(\vec{r})+V^t_0(x)\psi^0_{\vec{K}}(\vec{r})=E(\vec{K})\psi^0_{\vec{K}}(\vec{r})\ , \tag{1a}$$

where

$$V^t_0(x)=V^{ex}_{\vec{K}}(x)+V^{el}_0(x)\ . \tag{1b}$$

$V^{ex}_{\vec{K}}(x)$ denotes the exchange potential which is independent of y and z. It goes to zero as $x\to\infty$. It does depend on the wave numbers $\vec{K}$. The electrostatic part of the potential, $V^{el}_0(x)$, is calculated using the Poisson equation when the electronic charge density has been obtained from the electronic wave functions. We have

$$\begin{aligned}&\frac{d^2V^{el}_0(x)}{dx^2}=-4\pi e^2\rho_t(x)\ ,\\ &\rho_t(x)=\rho_0(x)-\rho_+ \quad \text{for } x<0\\ &\qquad=\rho_0(x) \qquad\quad \text{for } x>0\ .\end{aligned} \tag{2}$$

ρ_+ is the density of the positive background, and the free-electron density is given by

$$\rho_0(x)=2\sum_{\vec{K}}^{|\vec{K}|\le K_f}|\psi^0_{\vec{K}}(\vec{r})|^2\ . \tag{3}$$

The boundary conditions for the neutral metal are

$$V^{el}_0(x)=0,\quad \frac{dV^{el}_0}{dx}=0 \quad \text{for } x\to+\infty \tag{4a}$$

$$\frac{dV^{el}_0}{dx}=0 \quad \text{for } x\to-\infty\ . \tag{4b}$$

The constant value of V^{el}_0 in the interior gives the value of the dipole-layer potential energy. The energy eigenfunctions of Eqs. (1) can be written in the form

$$\psi^0_{\vec{K}}(\vec{r})=\frac{2^{1/2}}{L^{3/2}}\psi^0_k(x)e^{ik_2y+ik_3z}\ , \tag{5}$$

where L^3 is the volume of the metal. Inserting Eqs. (4) into Eqs. (1) one gets an equation for $\psi^0_k(x)$. Because $V^{ex}_{\vec{K}}(x)$ and $V^{el}_0(x)$ become constants ($A^0_{\vec{K}}$ and V^{el}_0, respectively) inside the metal, the asymptotic form of $\psi^0_k(x)$ inside the metal is given by

$$\psi^0_k(x)=\sin[kx-\varphi_0(k)] \quad \text{as } x\to-\infty\ . \tag{6}$$

$\vec{K}$ in Eq. (5) takes the values

$$k_2=(2\pi/L)m,\quad k_3=(2\pi/L)n,\quad m,n=0,\pm1,\pm2,\ldots$$

and $k=(\pi/L)l$, where l tends to positive integers as $L\to\infty$. The energy eigenvalue associated with $\psi^0_{\vec{K}}(\vec{r})$ is given by

$$E(\vec{K})=(\hbar^2/2m)(k^2+k_2^2+k_3^2)+V^{el}_0+A^0_{\vec{K}}\ . \tag{7}$$

When an external electric field is applied to a metal a charge density is induced at the metal surface which screens the interior of the metal from the external field. The potential barrier at the metal-vacuum interface changes accordingly. In principle the calculations of the new potential can be calculated self-consistently in exactly the same manner as for the neutral metal except that the boundary conditions (4a) must now be replaced by

$$\frac{dV^{el}}{dx}=F \quad \text{for } x\to\infty\ , \tag{8}$$

where V^{el} is the total electrostatic potential when the field F is applied.

We know, however, that to a first approximation the potential barrier outside the metal when a weak field is applied is given by

$$V^t_F(x)=V^t_0(x)+Fx\ . \tag{9}$$

Hence it is reasonable to assume that a proper calculation will result in a potential barrier of the form

$$V_F^t(x) = V_0^t(x) + Fx + \delta V(x) \ . \tag{10}$$

Moreover, one expects that $\delta V(x)$, because of the localization of the induced charge in a small region around $x = 0$ (see e.g., Fig. 4), will, at a reasonable distance (say, 2 Å or so) away from the metal surface, acquire the form

$$\delta V(x) \simeq F x_0(F), \quad x \gtrsim 2 \text{ Å} \tag{11}$$

so that

$$V_F^t(x) \simeq V_0^t(x) + F[x - x_0(F)] \ . \tag{12}$$

Fortunately, in most practical applications one requires knowledge of Eq. (12) rather than the full potential given by Eq. (10).

In field emission and field ionization the term Fx_0 is equivalent to an effective work-function change. x_0 will be referred to as the penetration length. In the remainder of this paper we attempt to evaluate the induced potential $V_F(x)$ as a function of the applied electric field and the neutral potential barrier $V_0^t(x)$. In our calculation we shall make the simplifying assumptions that $V_0^t(x)$ can be effectively replaced by an average potential barrier in the sense of Slater[11] which is independent of the wave number $\vec{K}$. This simplification is not as bad as it may appear at first sight. This has been demonstrated by Juretschke[12] and by other calculations[13] using the Kohn and Sham approach.[14] Moreover, the form and magnitude of the potential barrier $V_0^t(x)$ will be chosen on an empirical basis and *assumed* to be self-consistent.

We have done our calculations using two plausible forms for $V_0^t(x)$. Naturally the calculated $V_F(x)$ depends on the choice of $V_0^t(x)$ and this is a disadvantage in our calculation. However, the alternative of actually calculating $V_0^t(x)$ self-consistently, apart from being extremely laborious, could only result in a very approximate potential anyhow, because of our limited knowledge of correlation effects in the surface region. On the other hand, when we have done the calculation for two different neutral potential barriers we hope to be able to establish semiquantitatively the characteristics of the field-induced correction to the potential barrier (the metallic-field effect) and the order of magnitude of the field penetration. One also hopes to obtain some indication of the way different charge distributions react to the application of an external field.

The two forms for $V_0^t(x)$ used in our calculation are shown in Fig. 1. In both cases we have taken the constant value of the potential in the interior of the metal to be $V_0 = -10$ eV and the work function was taken equal to $\phi = 4.5$ eV. These parameters were taken to correspond to the free-electron model employed in studies of field emission from tungsten.[15] These two parameters automatically determine k_f, the wave number at the Fermi level, and hence the electron density in the interior of the metal, which is given by

$$\rho_c = k_f^3/3\pi^2 \ . \tag{13}$$

This value also gives the density of the uniform positive background. The first neutral potential barrier (broken line of Fig. 1) is given by

$$\begin{aligned} V_{01}^t(x) &= -(e^2/4x)(1 - e^{-lx}) \quad \text{for } x \geq 0 \\ &= V_0 + A e^{\mu x} \qquad\qquad \text{for } x \leq 0 \ . \end{aligned} \tag{14}$$

The parameters A and μ were determined from the continuity requirements for $V_0^t(x)$ and dV_0^t/dx at $x = 0$. The parameter l is determined by the requirement of over-all charge neutrality of the metal. The values of these parameters together with the estimated magnitude of the electric double-layer potential are given in the figure caption. The electronic charge density corresponding to the potential barrier of Eq. (14) is shown in Fig. 2 (broken line). It has been calculated using Eqs. (3) and (5) translated into an integral

$$\rho_0(x) = \frac{1}{\pi^2} \int_0^{k_f} (k_f^2 - k^2) \, |\psi_k^0(x)|^2 \, dk \ , \tag{15}$$

where $\psi_k^0(x)$ is obtained from the Schrödinger equation

$$-\frac{d^2\psi_k^0}{dx^2} + \frac{2m}{\hbar^2}[V_0^t(x) - V_0]\psi_k^0(x) = k^2 \psi_k^0(x) \ , \tag{16}$$

with $V_0^t(x)$ given by Eq. (14) and subject to the boundary conditions given by Eq. (4). The second neutral potential barrier employed in our calculations (solid line in Fig. 1) is given by

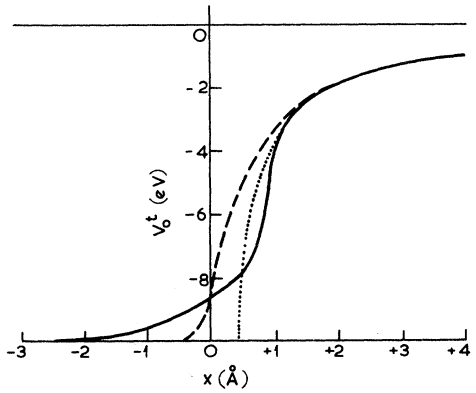

FIG. 1. Electron potentials V_{01}^t and V_{02}^t for the neutral metal used for the calculation of the induced potential $V_F(x)$. The image law (dotted line) is plotted for comparison. Broken line: $V_{01}^t(x) = -(e^2/4x)(1 - e^{-lx})$ for $x \geq 0$; $V_{01}^t(x) = V_0 + A e^{\mu x}$ for $x \leq 0$. ($A = 2.075$ eV, $l = 2.2$ Å^{-1}, $\mu = 8.7174$ Å^{-1}, $V_0 = -10$ eV, $V_{\text{double layer}} = 1.4$ eV.) Solid line: $V_{02}^t(x) = -e^2/4x$ for $x \geq 1$ Å; $V_{02}^t(x) = V_0 + (x^4 + Bx^3 + Cx^2 + Dx + E)^{-1}$ for $x \leq 1$ Å. ($B = -1.30703$, $C = 0.02696$, $D = 0.22070$, $E = 0.65703$, $V_0 = -10$ eV, $V_{\text{double layer}} = 3.58$ eV.)

$$V_{02}^{t}(x) = -e^2/4x \quad \text{for } x \geq 1 \text{ Å}$$
$$= V_0 + (x^4 + Bx^3 + Cx^2 + Dx + E)^{-1} \quad \text{for } x \leq 1 \text{ Å} . \tag{17}$$

The values of the parameters as determined from the continuity and charge neutrality requirements are given in the figure caption. The corresponding electronic charge density is shown in Fig. 2 (solid line).

We note that the oscillatory part of the neutral potential barrier has been neglected altogether. There is evidence[13] that these oscillations are greatly diminished because of the mutual cancellation of the electrostatic and exchange part of the potential. Once a $V_0^t(x)$ has been chosen and the corresponding $\rho_0(x)$ has been evaluated, we proceed with an approximate evaluation of the induced potential $V_F(x)$ as follows.

We start with an initial guess for $V_F(x)$. We then calculate the corresponding wave functions (the x-dependent part) from the Schrödinger equation:

$$-\frac{d^2\psi_k^F}{dx^2} + \frac{2m}{\hbar^2}\left[V_0^t(x) + V_F(x)\right]\psi_k^F(x) = E(k)\psi_k^F(x) , \tag{18a}$$

where

$$E(k) = (\hbar^2/2m)k^2 + V_0 , \tag{18b}$$

using entirely numerical techniques. In doing so we employed the De Volegaer method.[16] The initial values of the wave functions were specified, apart from a multiplicative constant which was subsequently normalized by the asymptotic form of the wave functions in the interior of the metal [see Eq. (6)], by using the WKB approximation at a distance sufficiently away from the metal surface. Thus, in the case of a positive field, the potential barrier the electron sees increases monotonically for $x \gg 0$ and the corresponding WKB wave function is given by

$$\psi_k^F(x) = \frac{c}{[V_F^t(x) - E(k)]^{1/4}} \times \exp\left[-\left(\frac{2m}{\hbar^2}\right)^{1/2}\int_{x_i}^{x}[V_F^t(x') - E(k)]\,dx'\right] \tag{19}$$

for $x \geq x_i$. We found that we could obtain accurate results by choosing $x_i \gtrsim 5$ Å.

When a negative electric field is applied electrons can tunnel through the resulting potential barrier (field emission) and in this case the asymptotic form of the WKB wave function to the right of the second classical turning point is given by

$$\psi_k^F(x) = \frac{c}{[E(k) - V_F^t(x)]^{1/4}} \times \exp\left[i\left(\frac{2m}{\hbar^2}\right)^{1/2}\int_{x_i}^{x}[E(k) - V_F^t(x')]\,dx'\right]$$

for $x \gtrsim x_i \gtrsim |E(k)/F|$. (20)

The Schrödinger equation (18a) is solved for a sufficient number of values of k to allow an accurate numerical evaluation of the density $\rho_F(x)$ obtained from Eq. (15) with $\psi_k^0(x)$ replaced by $\psi_k^F(x)$.

The induced charge density is then given by

$$\bar{\rho}_F(x) = \rho_F(x) - \rho_0(x) . \tag{21}$$

$V_F(x)$ in Eq. (18a) consists of two parts: an electrostatic part $V_F^{el}(x)$ and an exchange correlation part $V_F^{xc}(x)$. The electrostatic part is determined numerically from the Poisson equation

$$\frac{d^2V_F^{el}}{dx^2} = -4\pi e^2\bar{\rho}_F(x) \tag{22}$$

together with the boundary conditions

$$\frac{dV_F^{el}}{dx} = F \quad \text{for } x > x_i , \tag{23a}$$

$$\frac{dV_F^{el}}{dx} = 0 \quad \text{for } x \ll 0 . \tag{23b}$$

It should be noted that the total electrostatic potential satisfies the correct boundary conditions.

The exchange correlation modification to $V_0^t(x)$ induced by the electric field we could only estimate in a semiempirical manner using the following formula:

$$V_F^{xc}(x) = \frac{\rho_0(x)}{\rho_c}\left[V_0^t(x) - V_0^{el}(x)\right]\left[\left(\frac{\rho_F(x)}{\rho_0(x)}\right)^{1/3} - 1\right] , \tag{24}$$

where $V_0^{el}(x)$ is the electrostatic part of the neutral potential obtained from $\rho_0(x)$ and the Poisson's equation. Equation (24) originates from Slater's formula

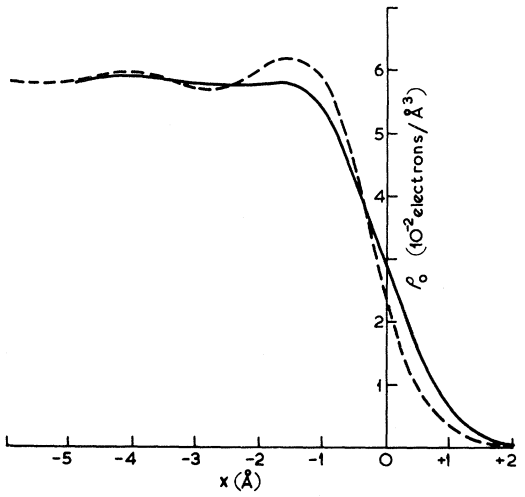

FIG. 2. Electron density $\rho_0(x)$ for the neutral metal. The broken line is calculated by using $V_{01}^t(x)$ as background potential and the solid line by using $V_{02}^t(x)$.

$$V^{ex}(x) = C\rho^{1/3} \tag{25}$$

by treating C as a function of x. Following Bardeen[10] we assume that the correlation can be effectively taken into account by considering it as a fraction of the exchange energy. Equation (25) overestimates[12] the exchange interaction in regions of small $\rho(x)$ which leads us to introduce $\rho_0(x)/\rho_c$ as a correction factor. In this way the exchange potential in the surface region looks more like the one calculated by more elaborate methods.[12] If the resulting induced potential $V_F(x) = V_F^{el}(x) + V_F^{xc}(x)$ calculated from Eqs. (22)–(24) is not the same as the input potential $V_F(x)$ used in Eq. (18), we try a different $V_F(x)$ and repeat the above procedure until we get a self-consistent result. Our numerical results obtained in this way for the two different neutral potentials given by Eqs. (14) and (17) are given in Sec. IV. In Sec. III we give an estimate of the "field penetration" $x_0(F)$ defined by Eq. (12) which avoids this lengthy numerical procedure. We must emphasize, however, that certain of the approximations involved in this calculation can be better understood when the results of the full numerical calculation are already known.

III. ESTIMATE OF THE "FIELD PENETRATION"

We proceed as follows. The asymptotic form of $\psi_k^F(x)$ satisfying Eq. (18) for $x \ll 0$, i.e., far inside the metal, is given by

$$\psi_k^F(x) = \sin[kx - \varphi_F(k)] \quad \text{as } x \to -\infty \ . \tag{26}$$

The following relation can be established:

$$\int_0^{k_f} k\,\varphi_F(k)\,dk = \tfrac{1}{8}\pi k_F^2 - (\pi/4e^2)F \ . \tag{27}$$

The proof of this relation for $F < 0$ is given in the Appendix. For $F > 0$, the proof is quite simple and for $F = 0$, Eq. (27) has been initially proved by Huntington[17] for a step-function potential and has been widely used in literature since then.

From Eq. (22) we get

$$\int_0^{k_f} k[\varphi_0(k) - \varphi_F(k)]\,dk = (\pi/4e^2)F \ . \tag{28}$$

We shall assume that the density $\rho_F(x)$ is given to a first-order approximation by

$$\rho_F(x) = \rho_0(x + \bar{\theta}) \ , \tag{29}$$

where $\bar{\theta}$ is an average of the displacement in the wave function because of the phase shifts:

$$\bar{\theta} = \int_0^{k_f} k^2\,\theta(k)\,dk \Big/ \int_0^{k_f} k^2\,dk = F/4\pi e^2\rho_c \ , \tag{30}$$

where

$$\theta(k) = [\varphi_0(k) - \varphi_F(k)]/k \ . \tag{31}$$

It is obvious from Eq. (29) that the induced electron density $\bar{\rho}_F(x)$, given by Eq. (21), is concentrated in the region where the derivative of $|\rho_0(x)|$ is large. This coincides with the surface region as expected (see also Fig. 4). Using Eqs. (22) and (23) together with Eqs. (21) and (29), we get

$$V_F^{el}(x) = F(x + \tfrac{1}{2}\bar{\theta}) + 4\pi e^2\bar{\theta}\int_x^{\infty} \rho_0(x')\,dx' - 4\pi e^2\int_x^{x+\bar{\theta}} \rho_0(x')(x - x' + \bar{\theta})\,dx' \ . \tag{32}$$

By noting that the second and third terms in Eq. (32) vanish away from the surface we get by comparison with Eq. (12)

$$x_0(F) = -\tfrac{1}{2}\bar{\theta} = -(1/8\pi e^2\rho_c)F \equiv \gamma F \ . \tag{33}$$

We note that Eq. (33) is valid for both positive and negative fields. The slope γ of $x_0(F)$ vs F is in good agreement with our numerical results.

IV. NUMERICAL RESULTS

In this section we present our numerical results obtained using the approximate method described in Sec. II. All numerical integrations were checked by halfing the step of integration until the desired accuracy was achieved. The starting point for the integration of the Schrödinger equation was chosen so as to introduce minimum error within the limitations of computing time available to us. The accuracy of this procedure was checked by varying the position of the starting point until no noticeable difference in the numerical results was found. The numerical integration was carried sufficiently far inside the metal to allow an accurate determination of the oscillatory part of the induced charge density and the corresponding potential. The initial value $V_F^{el}(x_1)$ and $dV_F^{el}(x_1)/dx$ of the electrostatic part of the induced potential were taken from their asymptotic forms which can be calculated from the asymptotic form of the wave functions. The accuracy was checked by shifting the point x_1 further into the metal so as to avoid errors larger than 10^{-3} eV to the potential.

Our results for the self-consistent induced charge density for two different values of the electric field are shown in Figs. 3 and 4. The broken line in Fig. 3 was calculated by omitting altogether the exchange correlation correction given by Eq. (24). The fact that the difference between the two is small indicates that a more elaborate treatment of exchange (and correlation) in this particular problem may not be worthwhile. In calculating $V_F(x)$ for the potential barrier given by Eq. (14) the exchange correction has been neglected altogether.

The self-consistent induced electric potential $V_F(x)$ for the two different neutral potential barriers is shown in Fig. 5 for a positive field and in Fig. 6 for a negative field. In Fig. 7, the corresponding total potential barrier is shown for a negative field appropriate to field emission in the region where high-field effects are observed experimentally (see Sec. V). In Fig. 8, we plot

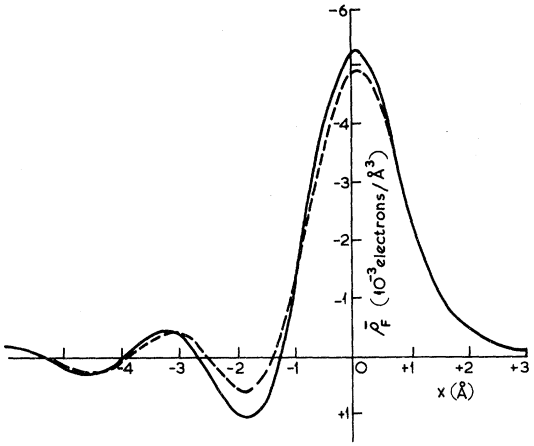

FIG. 3. Self-consistent induced electron density $\bar{\rho}_F(x)$ calculated by using background potential $V_{02}^t(x)$ and F =1.6 V/Å. The broken line was derived by using the Hartree calculation whereas the solid line by using the approximate Hartree-Fock calculation.

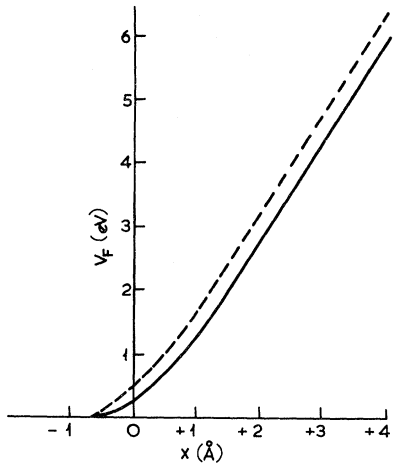

FIG. 5. Self-consistent induced electron potential $V_F(x)$ derived by employing the Hartree approximation and electric field $F=1.6$ eV/Å. The broken line was calculated by using background potential $V_{01}^t(x)$ and the solid line by using $V_{02}^t(x)$.

separately the electrostatic and exchange part of the field-induced potential for $F=1.6$ eV/Å. It is obvious from this figure that the exchange correction tends to eliminate the oscillatory part of the potential inside the metal in agreement with a similar conclusion of Lang[13] in relation to the neutral metal. This in a way justifies our neglecting these oscillations in the neutral potential barriers of Eqs. (14) and (17). In all numerical calculations we found that the dependence of the induced potential $V_F(x)$ on the externally applied field F can be put in the following form:

$$V_F(x)=F\,Y(x-\gamma F)\ , \tag{34}$$

where the function $Y(x)$ is independent of F. This functional relation was particularly helpful in the evaluation of the self-consistent potential for dif-

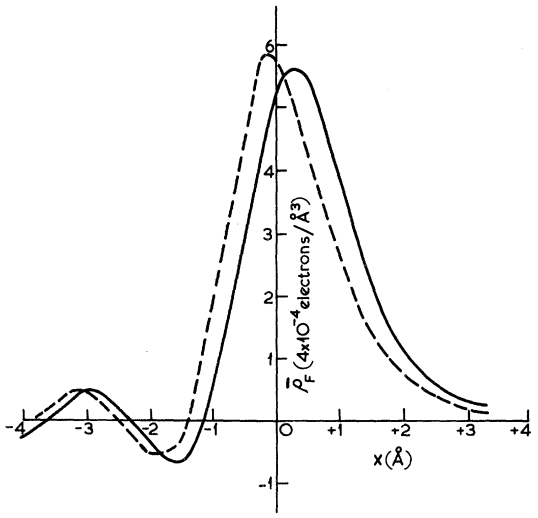

FIG. 4. Self-consistent induced electron density $\bar{\rho}_F(x)$ for $F=-0.8$ eV/Å, derived by employing the Hartree calculation. The broken line corresponds to background potential $V_{01}^t(x)$ and the solid line to $V_{02}^t(x)$.

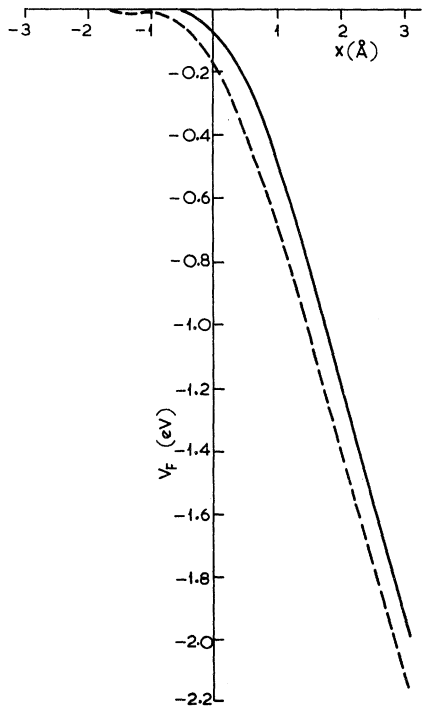

FIG. 6. Self-consistent induced electron potential $V_F(x)$ as calculated by the Hartree approximation for applied electric field $F=-0.8$ eV/Å. The broken line was calculated by using background potential $V_{01}^t(x)$ and the solid line by using $V_{02}^t(x)$.

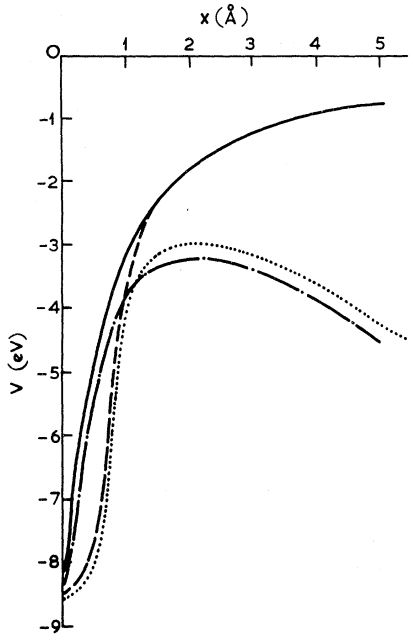

FIG. 7. Total potential barrier for $F=-0.8$ eV/Å. The neutral metal electron potentials are plotted for comparison. Solid line: $V_{01}^{t}(x)$; dot-dashed line: $V_{01}^{t}(x)+V_{F,1}(x)$; broken line: $V_{02}^{t}(x)$; dotted line: $V_{02}^{t}(x)+V_{F,2}(x)$.

ferent values of the field, once the self-consistent potential for a given field value had been established. The parameter γ remained constant for large positive fields ($F>1$ eV/Å). Its actual value was approximately -0.057 Å^2/eV for the first neutral potential barrier given by Eq. (14) and -0.08 Å^2/eV for the barrier given by Eq. (17) when the exchange correction was neglected. The value of the parameter γ remained the same with the exchange correction of Eq. (24) taken into account for the evaluation of $V_F(x)$, whereas the value of $x_0(F)$ increased by 0.1 Å for all fields. The above values compare reasonably well to the value of $\gamma=-0.05$ obtained from Eq. (33). The value of the "penetration" length $x_0(F)$ as defined by Eq. (12) and as determined from our numerical results is shown in Fig. 9. A striking feature of these curves and one which is not expected by our approximate formula (33) is the fact that $x_0(F)$ does not vanish for a zero field for either of the two neutral potential barriers used in our calculation. This fact is a direct consequence of our choosing the origin (arbitrarily) where the positive background charge of the metal ends abruptly. One can always take the origin (zero of the x axis) at $x_0(0)$ which is the "center of gravity" of the induced charge for $F\to 0$ and subsequently express the analytic formula giving the neutral potential barrier with respect to the new origin. The image

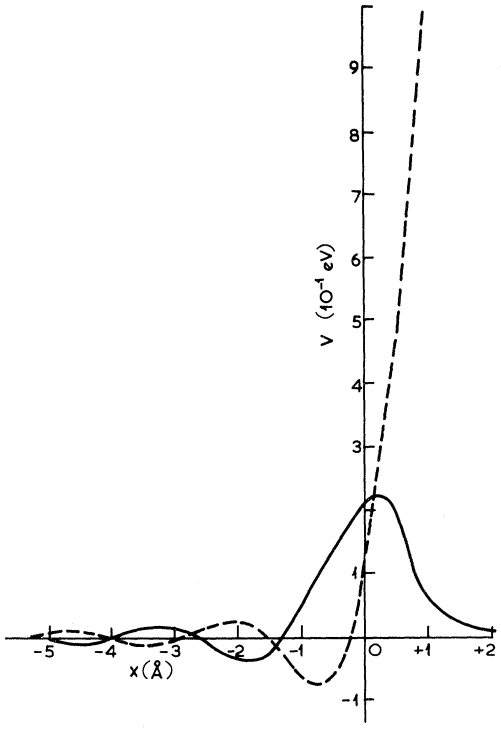

FIG. 8. Electrostatic part (broken line) and the exchange part (solid line) of the induced potential $V_F(x)$ derived by using background potential $V_{02}^{t}(x)$.

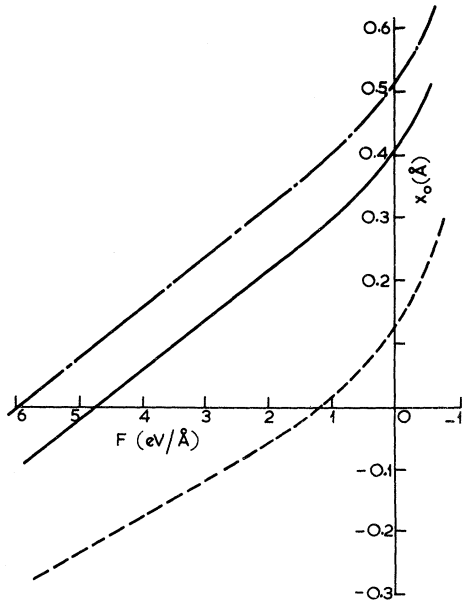

FIG. 9. Field penetration $x_0(F)$ vs F. The solid line was calculated by using the Hartree calculation and $V_{02}^{t}(x)$ as background potential. The dot-dashed line corresponds to the approximate Hartree-Fock calculation for the same potential. The broken line corresponds to the Hartree calculation for $V_{01}^{t}(x)$.

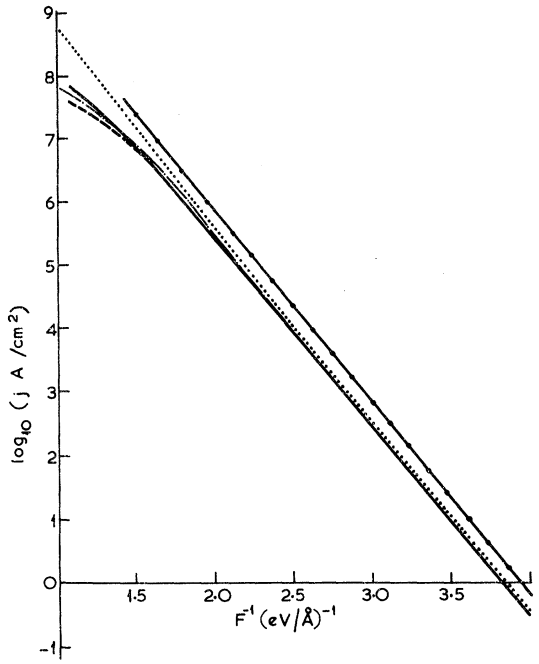

FIG. 10. $\log_{10} j$-vs-F^{-1} curves for the various calculations. Dotted line: Fowler-Nordheim theory; solid line: results of our calculation (metallic-field effect), when the space-charge effect was neglected. The results for the two background potentials used coincide in the figure. The broken line was calculated by correcting the solid line for the space-charge effect. The chainlike line shows the experimental results of Barbour and coworkers. The solid line with dots was calculated by neglecting the metallic-field effect altogether, i.e., by taking as potential barrier $V(x) = V_{02}^{+}(x) - |F|x$. For low fields the broken line and dot-dashed line coincide with the solid line.

law would still be valid asymptotically for $x \gg 0$ since

$$\frac{-e^2}{4x} = -\frac{e^2}{4[x' + x_0(0)]} \quad \text{(in old coordinates)}$$

$$= -\frac{e^2}{4x'} + \frac{x_0(0)e^2}{4x'^2} \quad \text{(in new coordinates)}. \tag{35}$$

It is worth noting that the new image plane at $x_0(0)$ is situated further to the right of the background positive charge edge for the neutral barrier given by Eq. (17) for which the electronic charge distribution stretches more out of the metal in comparison to the one corresponding to the potential barrier given by Eq. (14) (see, e.g., Fig. 2). It is also worth noting that the potential barrier as given by Eq. (35) is identical to the corrected image potential barrier for zero field as given by Sachs and Dexter.[18] The value of $x_0(0)$ according to Sachs and Dexter appropriate to the value of ρ_c that we used in the present calculation is approximately 0.41 Å and it is therefore in reasonable agreement with the values resulting from our calculation and Eq. (35).

The most important qualitative result for $x_0(F)$, as demonstrated in Fig. 9, is the fact that for a negative field (appropriate for field emission from a metal) $x_0(F)$ shifts outwards from the metal as the field increases in magnitude. According to the approximate equation (12) this increases the effective work function. This result is in qualitative agreement with the conclusions of Smith[19] who studied this problem using the Kohn-Sham approach. However, our detailed numerical evaluation of the current shows that this increase in the effective work function is very small to account for the difference (of about 0.6 eV) between the work function of certain crystallographic planes of tungsten as measured by field emission and thermionic emission, respectively. This is demonstrated in Fig. 10 where no noticeable change in the slope of the Fowler-Nordheim formula is observed except for very high fields. This is in agreement with a similar result obtained by Kaplit.[20] We note that the above result could not have been obtained with a boundary condition, such as $dV_F^{e1}/dx = 0$ at $x = 0$, which does not allow for the spread outwards of electronic charge at the metal-vacuum interface. We would also like to emphasize the obvious variation of $x_0(F)$ with the electric field in contrast with the corresponding result of Tsong and Muller[2] who find $x_0(F)$ as practically constant. We note that $Fx_0(F)$ of our equation (12) must be compared with $V(0) = F\lambda$ of Tsong and Muller [see Eqs. (17), (20), and (6) of their paper].

A noteworthy result of our calculation is the nonlinear response to the externally applied field. This is evident from Eq. (34) and the constant part of the asymptotic form of the potential Eq. (12) which according to our calculation (see Fig. 9) is

$$-Fx_0(F) = -Fx_0(0) - \gamma F^2 \ .$$

Of course, such a result could not be obtained by a linear response formalism.

V. APPLICATIONS

A. Field Emission

According to the Fowler-Nordheim (FN) theory[21] the current density of field emitted electrons is given by

$$j = \frac{aF^2}{\phi} \exp(-b\phi^{3/2}/|F|) \ , \tag{36}$$

where a and b are numerical constants and ϕ is the work function of the metal. A plot of $\log_{10} j$ vs $1/|F|$ gives a straight line which has been verified experimentally except for high fields ($F \gtrsim 5\times10^7$ eV/cm) where a deviation towards lower current densities is observed.[22] Equation (36) is evaluated

on the assumption that tunneling occurs through the barrier

$$V(x) = -e^2/4x - |F|x, \tag{37}$$

where F is determined from the applied potential V_{an} and the geometry of the cathode emitter (usually a hemispherical tip). One usually gets

$$F = \theta V_{an} , \tag{38}$$

where θ is simply a geometrical factor. Equation (38) is valid when space charge due to the emitted current is neglected. At high fields and hence large currents one cannot altogether neglect the space charge which results in a smaller effective field at the emitter surface and hence in a smaller current than that predicted by Eq. (36) with F given by Eq. (38). Barbour and his co-workers attributed the deviation of the $\log_{10} j$ vs $1/F$ from the FN plot entirely to space-charge effects. Other authors[23,24] attribute the high-field deviation from the FN plot to the inadequacy of the image law at small distances from the surface and they suggest that replacement of the first term in Eq. (37) by the improved version [see Eq. (35)] suggested by Sachs and Dexter can explain at least partly the observed deviation at high fields. A nonquantum correction to the image law has also been suggested,[25] due to surface irregularities, which, however, tends to cancel partly the effect of the quantum correction. We note that in all the analyses mentioned above the transmission coefficient is calculated by the WKB approximation. It is possible that this approximation overestimates the tunneling probability for thin barriers (i.e., high fields) in which case Eq. (36), itself calculated by the WKB, overestimates the current at high fields. In this case the observed deviation will be partly due to a calculational error. In order to avoid this possibility we calculated the field-emitted current density entirely numerically for the total self-consistent potential barrier, formally given by Eq. (10). We recall that this barrier depends on our choice of the neutral potential barrier and the electric field. It takes into account both the zero-field correction to the image law and the metallic-field effect. Since $\xi(F) = x_0(F) - x_0(0)$ is positive in the present case it is equivalent [see Eq. (12)] to an increase in the effective work function for high fields and could be an extra factor contributing to the experimentally observed deviations at high field. This is contrary to the conclusion of Sidyakin[3] who finds $\xi(F)$ negative in which case the metallic-field effect would tend to produce a higher current. According to Sidyakin this is neutralized by the quantum correction [second term in Eq. (35)] of the image law. In Table I we give $\log_{10} j_{FN}/j$ for the two different neutral potential barriers used in our calculation for different values of the electric field. j_{FN} is the Fowler-Nordheim value and j is the result of our numerical calculation. We observe that the results for the two cases are practically identical. This remains true for the total energy distribution (see e.g., Fig. 11). Thus, the measurable quantities, current density and TED are not very sensitive to the detailed structure of the potential barrier when the self-consistent potential is calculated according to our approach. This can be seen by the dotted solid line of Fig. 10 where the current was calculated without calculating self-consistently the potential, but taking it simply as $V_{02}^t(x) + Fx$. Since the neutral metal potential $V_{02}^t(x)$ (see Fig. 2, solid line) was chosen so as to result in a more transparent potential when the external potential $-|F|x$ is added, the $\log_{10} j$-vs-F^{-1} curve differs significantly from the FN curve. When the calculation was carried out with the total potential $V_{02}^t(x) + F[x - x_0(0)]$ the $\log_{10} j$-vs-F^{-1} curve deviated only slightly from the FN law.

As it can be seen by Table I the logarithms of the currents obtained by the self-consistent calculation for the two different neutral potentials differ

TABLE I. Logarithms of the current density j (j in A/cm^2) for various values of the electric field F. The values of $\log_{10} j$ obtained for $V(x) = V_0^t(x) + Fx$ are included for comparison. The space-charge correction is not included.

	Background potential					
		V_{01}^t			V_{02}^t	
$\|F\|$ (eV/Å)	Fowler-Nordheim theory	Self-consistent calculation	$V(x) = V_{01}^t(x) + Fx$	Self-consistent calculation	$V(x) = V_{02}^t(x) + Fx$	$V(x) = V_{02}^t(x) + F[x - x_0(0)]$
	$\log_{10} j$	$\log_{10} j$	$\log_{10} j$	$\log_{10} j$	$\log_{10} j$	$\log_{10} j$
0.25	−0.39	−0.665	−0.42	−0.611	−0.152	−0.546
0.5	5.59	5.283	5.562	5.32	5.848	5.44
0.7	7.36	7.000	7.33	7.04	7.619	7.214
0.8	7.94	7.51	7.90	7.55		7.777

only slightly so that in Fig. 10 they are drawn as one curve (broken line). The same holds when only the metallic field (i. e., without the space-charge correction) was taken into account (solid line in Fig. 10).

One would expect that the normal energy distribution should be more sensitive to the detailed structure of the barrier but unfortunately it has not yet been possible to obtain experimentally. We observe from Fig. 10 that when only the metallic field is taken into account the $\log_{10}j$-vs-F^{-1} plot resulting from our calculation (solid line) is displaced slightly downwards in relation to the FN plot. This is equivalent to a small change in the preexponential term of Eq. (36) which is always very difficult to determine accurately from experiment. A small deviation towards lower currents occurs at high fields (see Table II), but it is not sufficient to explain the experimentally observed one. However, when the space charge was taken into account the resulting curve (broken line on Fig. 10) gives sufficiently large deviations from the FN theory so as to explain the experimental results of Barbour and co-workers[22] which are exhibited by the chainlike line of Fig. 10.

By comparing the various curves in Fig. 10 we conclude that the experimentally observed deviation from the FN plot at high field is basically due to space-charge effects and to a lesser degree to the quantum correction of the image law and the metallic-field effect.

B. Field Ionization

In this case our results are qualitatively similar to those of Tsong and Muller.[2] $\xi(F)$ is negative and hence leads to a smaller critical metal-atom distance for field ionization. A smaller critical distance results in increased ion current and a narrower energy distribution in comparison with the result one obtains by neglecting field penetration altogether. This conclusion is in qualitative agreement with experimental observation. For values of the field appropriate to field ionization ($F > 1.5$ eV/Å), $|\xi(F)|$ is of the order of 0.5 Å which is in agreement with the result of Tsong and Muller who take $\lambda = 0.5$ Å for tungsten. For lower fields the calculation of Tsong and Muller overestimates the field penetration according to our calculation.

TABLE II. Values of $\log_{10}(j_{FN}/j)$, where j is the value of the current density obtained by our calculation.

$\|F\|$ (eV/Å)	$\log_{10}(j_{FN}/j)$ Values for V_{01}^t	Values for V_{02}^t
0.25	0.275	0.221
0.5	0.307	0.27
0.7	0.36	0.32
0.8	0.43	0.40

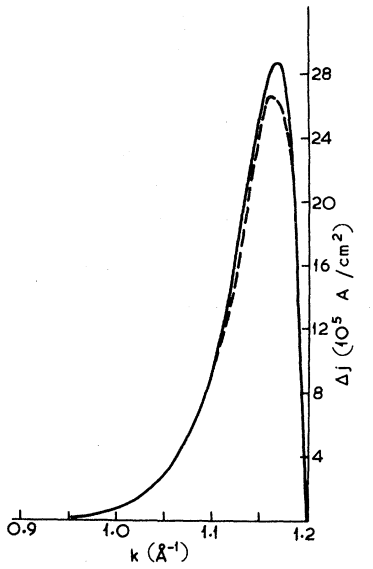

FIG. 11. Total energy distribution of emitted electrons for applied field $F = -0.7$ eV/Å. The plot is vs $k = [(2m/\hbar^2) \times (E - V_0)]^{1/2}$.

C. Capacitance of a Parallel-Plate Capacitor

The capacitance per unit area of a parallel-plate capacitor is given by

$$C = F_0/4\pi V , \tag{39}$$

where $F_0/4\pi$ is the surface charge density and V the potential difference which when the metallic-field effect (field penetration) is taken into account is approximately given by

$$V = \phi_1/l + [x_0^{(1)}(F) + t + x_0^{(2)}(F)]F_0 - \phi_2/l , \tag{40}$$

where ϕ denotes the work function and t the distance between the electrodes. The indices 1 and 2 refer to the two electrodes, respectively. According to our calculation $x_0^{(1)}(F)$ and $x_0^{(2)}(F)$ have opposite signs and hence practically cancel each other, hence the effect of "field penetration" on the capacitance is negligible according to our calculation. This is in qualitative agreement with the arguments of Mott and Watts-Tobin,[26] and it is contrary to the result of both Tsong and Muller[2] and Ku and Ullman.[4] According to these authors $x_0^{(1)}(F)$ and $x_0^{(2)}(F)$ have the same sign so that when $x_0^{(1)}(F) + x_0^{(2)}(F)$ becomes comparable to t, the capacitance should be modified according to Eq. (40). As we have already mentioned this difference results because the above authors assume an abrupt termination of the electronic charge distribution at the metal-vacuum

interface. Similar considerations apply to the case of a dielectric sandwiched between two metal electrodes. In that case F_0 is replaced in Eq. (40) by F_0/ϵ. where ϵ is the dielectric constant. If our conclusion is right the explanation of the observed deviation from the geometrical capacitance in metal insulator-metal sandwiches based on field penetration of the electrodes must be seriously reexamined. The same comment applies to a similar analysis of tunneling data[5,6] using the field-penetration model of Ku and Ullman.[4]

APPENDIX

We shall show that the relation

$$\int_0^{k_f} k\varphi_F(k)\,dk = \frac{\pi}{8}\,k_f^2 - \frac{\pi}{4e^2}\,F - \int_0^{k_f} \frac{(k_f^2-k^2)k(2m/\hbar^2)F\sin 2\theta\,dk}{8\{k_f^2+(2m/\hbar^2)[V_0-V(\xi)]\}^{5/2}} \quad \text{(A1)}$$

holds for negative fields, when the asymptotic form of the potential for large x is $-|F|\cdot(x-x_0)$ and $F=dV/d\xi$, where ξ is a point in the interval $(V_0/F, 2V_0/F)$.

Proof

The solution of the Schrödinger equation for $x \ll 0$, where the potential $V(x)$ assumes its constant value V_0 can be written in the following form:

$$\psi_k(x) = e^{i\alpha}\{\cos\theta\sin[kx-\varphi_F(k)] - i\sin\theta\cos[kx-\varphi_F(k)]\}\ . \quad \text{(A2)}$$

For $\xi,\ \xi_1 > [(\hbar^2/2m)k^2+V_0]/F$, the solution is

$$\psi_k(\xi) = \frac{k^{1/2}T^{1/2}}{[k^2-u(\xi)]^{1/4}}\exp\left\{i\int_{\xi_1(k)}^{\xi}[k^2-u(x)]^{1/2}dx\right\}, \quad \text{(A3a)}$$

where

$$T = \tfrac{1}{2}\sin 2\theta\ , \quad \text{(A3b)}$$

$$u(x) = (2m/\hbar^2)[V(x)-V_0]\ . \quad \text{(A3c)}$$

By a proper choice of the point $\xi_1(k)$ the phase factor $e^{i\alpha}$ in (A2) can be set equal to unity.

The following relation for the wave functions $\psi_k(x)$ and $\psi_{k'}(x)$ can be easily established:

$$\left(\psi_{k'}^*(x)\frac{d\psi_k}{dx} - \psi_k(x)\frac{d\psi_{k'}^*}{dx}\right) - \left(\psi_{k'}^*(\xi)\frac{d\psi_k}{d\xi} - \psi_k(\xi)\frac{d\psi_{k'}^*}{d\xi}\right) = (k^2-k'^2)\int_x^{\xi}\psi_{k'}^*(x')\psi_k(x')\,dx'\ . \quad \text{(A4)}$$

By noting that the Wroskian $W(x)$ is

$$W(x) = \psi_k^*(x)\frac{d\psi_k}{dx} - \psi_k\frac{d\psi_k^*}{dx} = ik\sin 2\theta(k) \quad \text{(A5)}$$

and subtracting $W(x)$ from both terms in the parentheses in Eq. (A4), we can modify this equation so that it is allowable to divide both sides by $(k^2-k'^2)$ and take the limit as $k'\to k$. The result is

$$G_F(k,\xi) - G_F(k,x) = \int_x^{\xi}|\psi_k(x')|^2dx'\ , \quad \text{(A6a)}$$

where

$$G_F(k,x) = \frac{1}{2k}\left(\frac{\partial\psi_k^*(x)}{\partial k}\frac{\partial\psi_k(x)}{\partial x} - \psi_k(x)\frac{\partial^2\psi_k^*(x)}{\partial x\partial k}\right)\ . \quad \text{(A6b)}$$

By using Eq. (A2) the first term of Eq. (A6a) for $x\to-\infty$ can be calculated. The result is

$$G_F(k,x) = -\frac{1}{4k}\cos 2\theta\sin 2[kx-\varphi_F(k)] + \frac{1}{2}\left(x-\frac{d\varphi_F}{dk}\right). \quad \text{(A7)}$$

For $\xi > V_0/F$, we get, by inserting Eq. (A3) into Eq. (A6b),

$$G_F(k,\xi) = \frac{k}{8}\sin 2\theta\frac{du}{d\xi}\frac{1}{[k^2-u(\xi)]^{5/2}} - \sin 2\theta\frac{\partial}{\partial k}\int_{\xi_1(k)}^{\xi}[k^2-u(x)]^{1/2}dx\ , \quad \text{(A8)}$$

but

$$\frac{\partial}{\partial k}\int_{\xi_1(k)}^{\xi}[k^2-u(x)]^{1/2}dx = \int_{\xi_1(k)}^{\xi}\frac{k\,dx}{[k^2-u(x)]^{1/2}} - \frac{d\xi_1(k)}{dk}\{k^2-u[\xi_1(k)]\}^{1/2}\ . \quad \text{(A9)}$$

Since the choice of $\xi_1(k)$ is such that the phase factor $e^{i\alpha}$ in Eq. (A2) is unity, and the wave function for $\xi > V_0/F$ is rapidly oscillating, a point $\xi(k)$ can be found in the region $(V_0/F,\ 2V_0/F)$ so that the right-hand side of Eq. (A9) is equal to 0, then

$$\int_0^{k_f}dk(k_f^2-k^2)\int_x^{\xi(k)}|\psi_k(x')|^2dx' = \int_0^{k_f}dk(k_f^2-k^2)\frac{\sin 2\theta(du/d\xi)}{[k^2-u(\xi)]^{5/2}} + \int_0^{k_f}dk\,(k_f^2-k^2) \times\left[\frac{1}{4k}\cos 2\theta\sin\{2[kx-\varphi_F(k)]\} - \frac{1}{2}\left(x-\frac{d\varphi_F}{dk}\right)\right]. \quad \text{(A10)}$$

But since all points $\xi(k)$ are in the region $(V_0/F,\ 2V_0/F)$ an average $\bar{\xi}$ can be found lying in this region so that

$$\int_0^{k_f}dk(k_f^2-k^2)\int_x^{\bar{\xi}}|\psi_k(x')|^2dx' = \int_0^{k_f}dk\,(k_f^2-k^2)\int_x^{\xi(k)}|\psi_k(x')|^2dx'\ . \quad \text{(A11)}$$

By taking into account the relation

$$4\pi e^2\int_x^{\bar{\xi}}[\rho(x')-\rho_c H(-x')]\,dx' = \frac{dV}{d\xi} = F\ , \quad \text{(A12)}$$

where $H(x)$ is the Heaviside function, we find, after calculating the integrals in Eq. (A10) for $x\to-\infty$,

$$\int_0^{k_f} k\varphi_F(k)\,dk = \frac{\pi}{8}k_f^2 - \frac{\pi}{4e^2}F - \frac{2m}{\hbar^2}F\int_0^{k_f}\frac{(k_f^2-k^2)k}{8} \times \frac{\sin 2\theta\,dk}{\{k^2+(2m/\hbar^2)[V_0-V(\xi)]\}^{5/2}} \quad . \quad (A1')$$

For the fields and electron densities of interest the term under the integral sign on the right-hand side of Eq. (A1) is very small. In addition, the charge density in the region $(V_0/F,\ 2V_0/F)$ is practically zero so that in applications the choice of the average point is not of any significance. Therefore, Eq. (A1) for all practical applications is identical to the equation for positive fields.

[1]R. Gomer and L. W. Swanson, J. Chem. Phys. 38, 1613 (1963).

[2]T. T. Tsong and E. W. Muller, Phys. Rev. 181, 530 (1969).

[3]A. V. Sidyakin, Zh. Eksperim. i Teor. Fiz. 58, 573 (1970) [Sov. Phys. JETP 31, 308 (1970)].

[4]H. Y. Ku and F. G. Ullman, J. Appl. Phys. 35, 265 (1964).

[5]J. Simmons, Phys. Letters 16, 233 (1965).

[6]J. Simmons, Phys. Letters 17, 104 (1965).

[7]R. Stratton, Proc. Phys. Soc. (London) B68, 746 (1955).

[8]D. M. Newns, Phys. Rev. B 1, 3304 (1970).

[9]J. A. Applbaum and G. A. Baraff, Phys. Rev. B 4, 1246 (1971).

[10]J. Bardeen, Phys. Rev. 49, 653 (1936).

[11]J. C. Slater, *Quantum Theory of Matter* (McGraw-Hill, New York, 1968), pp. 336–344.

[12]H. J. Juretschke, Phys. Rev. 92, 1140 (1953).

[13]J. R. Smith, Phys. Rev. 181, 522 (1969); N. D. Lang, Solid State Commun. 7, 1047 (1969); N. D. Lang and W. Kohn, Phys. Rev. B 1, 4555 (1970).

[14]W. Kohn and L. J. Sham, Phys. Rev. 140, A1133 (1965).

[15]P. H. Cutler and J. J. Gibbons, Phys. Rev. 111, 394 (1958).

[16]See, for example, R. A. Buckingham, *Numerical Methods* (Pitman, London, 1962), p. 244.

[17]H. B. Huntington, Phys. Rev. 81, 1035 (1951).

[18]R. G. Sachs and D. L. Dexter, J. Appl. Phys. 21, 1304 (1950).

[19]J. R. Smith, Phys. Rev. Letters 25, 1023 (1970).

[20]M. Kaplit, *Thermionic Conversion Specialist Conference, Houston* 1966 (IEEE, New York, 1967), pp. 387–94.

[21]R. Gomer, *Field Emission and Field Ionization* (Harvard U. P., Cambridge, Mass., 1961), Chaps. 1 and 3.

[22]J. P. Barbour, W. W. Dolan, J. K. Trolan, E. E. Martin, and W. P. Dyke, Phys. Rev. 92, 45 (1953); see also, W. P. Dyke and J. K. Trolan, *ibid.* 89, 799 (1953).

[23]T. J. Lewis, Proc. Phys. Soc. (London) B68, 938 (1955); Phys. Rev. 101, 1694 (1956).

[24]P. H. Cutler and D. Nagy, Surface Sci. 3, 71 (1964).

[25]A. Modinos, Surface Sci. 9, 459 (1968).

[26]N. F. Mott and R. J. Watts-Tobin, Electrochim. Acta 4, 79 (1961).